IAC–19–C2.7.1

Boundary Layer Stability and Laminar-Turbulent Transition Analysis with Thermochemical Nonequilibrium Applied to Martian Atmospheric Entry

H.L. Kline
Research Engineer, Research Department, National Institute of Aerospace, Hampton, VA, 23666, USA, heather.kline@nianet.org

C-L. Chang
Aerospace Technologist, Computational Aerosciences Branch, MS 128, NASA Langley Research Center, USA, chau-lyan.chang@nasa.gov

F. Li
Aerospace Technologist, Computational Aerosciences Branch, MS 128, NASA Langley Research Center, USA, fei.li@nasa.gov

As Martian atmospheric entry vehicles increase in size to accommodate larger payloads, transitional flow may need to be taken into account in the design of the heat shield in order to reduce heat shield mass. The mass of the Thermal Protection System (TPS) comprises a significant portion of the vehicle mass, and a reduction of this mass would result in fuel savings. The current techniques used to design entry shields generally assume fully turbulent flow when the vehicle is large enough to expect transitional flow, and while this worst-case scenario provides a greater factor of safety it may also result in overdesigned TPS and unnecessarily high vehicle mass. Greater accuracy in the prediction of transition would also reduce uncertainty in the thermal and aerodynamic loads. Stability analysis, using e^N-based methods including Linear Stability Theory (LST) and the Parabolized Stability Equations (PSE), offers a physics-based method of transition prediction that has been thoroughly studied and applied in perfect gas flows, and to a more limited extent in reacting and nonequilibrium flows. These methods predict the amplification of a known disturbance frequency and allow identification of the most unstable frequency. Transition is predicted to occur at a critical amplification or N Factor, frequently determined through experiment and empirical correlations. The LAngley Stability and TRansition Analysis Code (LASTRAC), with modifications for thermochemically reacting flows and arbitrary gas mixtures, will be presented with LST results on a simulation of a high enthalpy CO_2 gas wind tunnel test relevant to Martian atmospheric entry. The results indicate transition caused by modified Tollmien-Schlichting waves on the leeward side, which are predicted to be more stable and cause transition slightly downstream when thermochemical nonequilibrium is included in the stability analysis for the same mean flow solution.

keywords: transition, boundary-layer stability, thermochemical nonequilibrium, reentry, Mars, transition

Nomenclature

F nondimensionalized frequency.

T_V vibrational-electronic temperature [K].

T_e boundary layer edge temperature [K].

α complex wave number.

β disturbance spanwise wave number.

ω disturbance streamwise wave number.

ϕ disturbance vector.

ρ_e boundary layer edge density [kg m^{-3}].

u_e boundary layer edge velocity [m s^{-1}].

Abbreviations

CNE Chemical Nonequilibrium with Thermal Equilibrium.

CP Calorically Perfect.

CTE Chemical and Thermal Equilibrium.

DNS Direct Numerical Simulation.

LASTRAC LAngley Stability and TRansition Analysis Code.

LST Linear Stability Theory.

NPSE Nonlinear PSE.

PSE Parabolized Stability Equations.

TNE Thermochemical Nonequilibrium.

TPS Thermal Protection System.

1. Introductions

Prediction of heat transfer rates and integrated heat loads inform the design of the Thermal Protection System (TPS), which significantly impacts the mass of reentry vehicles, planetary probes, and Martian entry vehicles. Reducing this mass has benefits in terms of decreased fuel requirements and increased payload; however, due to the high risk and uncertainty, the TPS or heat shield is often designed conservatively assuming fully turbulent flow. The Mars 2020 entry shield design, for example, is evaluated as fully turbulent [1]. Laminar flow results in reduced heat flux, and so more accurate and reliable prediction of transition should result in more efficient vehicle design. The potential benefits of a greater understanding of hypersonic boundary layer transition are significant. Analysis of the National AeroSpace Plane (NASP) aerodynamics [2] estimated that the possible payload of an air-breathing single-stage-to-orbit vehicle would double if it was fully laminar as compared to fully turbulent. Techniques to control transition include wall cooling, which is effective in stabilizing the first Mack mode but destabilizing to the 2nd Mack mode [3, 4].

The literature on boundary layer stability in the hypersonic regime includes both studies focusing on the instabilities neglecting the effects of chemical reactions and use Calorically Perfect (CP) assumptions [5–9], as well as experimental studies that use sufficiently low temperatures to avoid significant chemical reactions [10, 11]. Johnson et al. [12–14] address three-dimensional Parabolized Stability Equations (PSE) solutions with Thermochemical Nonequilibrium (TNE) with their STABL-3D code. TNE boundary layer stability is also addressed by Bertolotti [15] and by Wang et al. [16] with Local, or Linear Stability Theory (LST), and by Knisely and Khong [17] with Direct Numerical Simulation (DNS). Studies, which neglect thermal nonequilibrium and use only Chemical Nonequilibrium with Thermal Equilibrium (CNE) or Chemical and Thermal Equilibrium (CTE), have also included Nonlinear PSE (NPSE) [5] and PSE [18–20] can also be found in the literature. Experimental results at high-enthalpy conditions where thermochemical effects are expected to be significant include work described in Wartemann et al. [21] for sharp cones, and by Hollis et al. [11, 22] for the MSL aeroshell. Kimmel [3] provides a thorough review of hypersonic transition control techniques, and states that one of the difficulties of hypersonic transition control is that the techniques applied at lower speeds cannot be extrapolated to the high heating environment and the physical phenomena occurring within these boundary layers.

Although transition was demonstrated in wind-tunnel tests [11], flight data [23], and numerical studies [9, 24], uncertainty in the transition location was held to be high enough that the TPS should be designed for fully turbulent flow, and therefore, greater mass than would have been required for a partially-laminar TPS design. Edquist et al. [25] conducted detailed computational studies of the MSL aeroshell, focusing on thermal and chemical nonequilibrium with a five-species gas mixture, using Park [26] reaction rates and using a critical value of momentum-thickness Reynolds number. The peak turbulent heating rate was predicted to be 70% higher than the heating rate for laminar flow, with a fully turbulent shield experiencing 38% higher integrated heat load as compared to the fully laminar case.

Experimental and computational work has been done investigating a stabilizing effect of CO_2 injection into high enthalpy boundary layers for delay of transition [27–29], due to the characteristic of CO_2 to absorb energy at frequencies close to the 2nd Mack mode. Given the results available in literature and in previous work by the authors, thermochemical nonequilibrium and CO_2 are expected to be stabilizing to the boundary layer and delay transition.

Previous work by Kline et al. [30–32] details the development of thermochemical nonequilibrium capabilities for LASTRAC [33]. LASTRAC is a boundary-layer stability analysis code that provides PSE as well as LST to predict the stability of a boundary layer and transition with semiempirical e^N methods. The thermochemical capabilities have since been extended to three-dimension geometries. While further investigation on the effects of the chemical model are outside the scope of this work, it is has been shown that nonequilibrium chemistry is sensitive to the models used, and that boundary layer stability specifically is sensitive to vibrational energy relaxation as shown by Bertolotti [15]. The thermochemistry models used here are similar to those used generally in Computational Fluid Dynamics (CFD)

for mean flows and with those used in previous studies of boundary layer stability; more advanced and recently-developed models such as state-to-state models will not be addressed here. The code used in this work has been developed with the intention of being compatible with any user-provided chemical model, such that the effects of using these models might be included in the future.

In this work, we perform instability analysis on an MSL geometry under wind tunnel conditions, which were reported to produce transitional flow. Hollis et al. [11] compared laminar, transitional, and turbulent heating data on the MSL entry vehicle in an air wind tunnel and a high-enthalpy shock tunnel with CO_2 gas, and compared results to Navier-Stokes solutions. Using laminar CFD solutions, they produced transition location correlations based on boundary layer momentum thickness, edge Mach number, and Reynolds number based on momentum thickness. Selected cases from these wind tunnel tests have been analyzed with the Langley Stability and Transition Analysis Code (LASTRAC) [33] by Chang et al. [9] with air only and PSE-Chem by Johnson et al. [24] at 0° angle of attack in air, with initial analysis provided for a CO_2 case. Further work by Hollis et al. [22, 34] continued work for high-enthalpy CO_2 gas mixtures, and in communication with the authors, the results from this work may be more reliable than their prior work [11] due to unsteady conditions encountered, although both are subject to questions of flow quality.

1.1 *Geometry & Conditions*

The LENS-XX shot 18 case from Hollis et al. [34] was identified as including transitional flow. The nominal flow conditions were pure CO_2 gas, with freestream velocity of 2021 m/s, freestream temperature of 140 K, freestream pressure of 614 Pa, freestream density of 2.32×10^{-2} kg/m^2, freestream Mach number of 10.7, and angle of attack of 16°. A noncatalytic and isothermal wall boundary condition was used with a wall temperature of 300 K. The model used in wind-tunnel tests was an 8-in. diameter 70 degree sphere-cone model similar to the Mars Science Laboratory (MSL) entry vehicle and described more fully in Hollis et al. [22, 34].

2. Theory and calculation

Section 2.1 will describe the PSE and LST methods, followed by a description of the chemical model in Section 2.2 and mean flow solutions in Section 2.3.

2.1 *Boundary Layer Stability Analysis*

LASTRAC includes capabilities to analyze boundary layer stability with LST and PSE. These methods assume a disturbance vector solution that is a discrete sum of a Fourier series. The LST method assumes that the boundary layer is nearly parallel, with negligible growth of the thickness of the boundary layer, and uses a mode shape, or perturbation form, for the Fourier series that has a shape function and wave number that are locally constant in the streamwise direction. For the PSE, the assumed mode shape uses a shape function and wave number that vary slowly in the streamwise direction. While an eigenvalue problem is formed in the LST approach, the PSE method numerically solves an approximate form of the governing partial differential equations for the slow-varying shape function with an actively updated wave number along the streamwise direction. The nonlinear PSE uses a mode shape similar to the PSE, but retains nonlinear terms from the Navier-Stokes equations, and requires a known finite disturbance while both LST and linear PSE are independent of the input disturbance amplitude but only valid for sufficiently small disturbances. LASTRAC was modified to include further capabilities for high-enthalpy hypersonic applications by Kline et al. [30, 31]. Further details on the capabilities previously available in LASTRAC are available in the LASTRAC manual [33]. Previous work [31] includes more complete details of the modifications required to accommodate gas chemistry effects. Three-dimensional marching techniques used in this work are described by Chang [35].

Stability equations are derived starting from the nondimensionalized Navier-Stokes equations. For this application they are nondimensionalized by the boundary layer edge values: ρ_e, T_e, and u_e. A body-fitted coordinate system is used where x, y, and z are defined as streamwise, wall-normal, and spanwise, respectively. Perturbations to the mean flow quantities are expressed in terms of the disturbance vector $\phi = \{p', u', v', w', T'\}^T$. The disturbance field ϕ is assumed to be periodic in space and time, and so the disturbance vector can be expressed as a Fourier series,

$$\phi(x, y, z, t) = \sum_{m=-M}^{M} \sum_{n=-N}^{N} \chi_{mn}(x, y) e^{i(n\beta z - m\omega t)}, \quad [1]$$

where M and N represent the numerical resolution in time and space, respectively. Substituting a single disturbance mode defined by the streamwise wave

number $\omega = \frac{2\pi\ell}{u_e} f$ and spanwise wave number $\beta = \frac{2\pi}{\lambda_z}$ results in the Linearized Navier-Stokes (LNS) equations.

This system can be solved numerically, and simplifications lead to approximate solutions that are obtained at a lower computational cost for engineering applications. One such simplification is the quasiparallel assumption that neglects the velocity normal to the wall and all mean flow variation in the x direction. The linear PSE decomposes the mode shape into two parts: a complex wave number α that varies only in x and a shape function that varies in x, y, and z,

$$\chi = \hat{\chi}(x,y,z) e^{i \int_{x_0}^{x} \alpha(\xi,z) d\xi + \int_{z_0}^{z} \beta(x,\eta)} , \qquad [2]$$

where ξ is the variable of integration. The linear PSE neglects the products of disturbances, or 2^{nd}- and higher-order perturbations. Another possible simplification is the quasiparallel assumption that neglects velocity normal to the wall and all mean flow variation in the x direction, where χ is a function of y only, leading to the LST solutions. This process is repeated separately for the CP, CTE, CNE, and TNE models. The line-marching PSE used in this work assumes negligible spanwise mean flow variation and a real-valued β.

The methods described above to solve for ϕ produce results presented in terms of a nondimensional frequency F, the complex part of the wavenumber α_i, and the N-Factor based on disturbance kinetic energy,

$$\begin{aligned} F &= \frac{2\pi\ell}{u_e} f \\ \alpha_i &= \Im\left(\alpha(x)\right) \\ E &= \int_0^{y_e} \rho(|u'|^2 + |v'|^2 + |w'|^2) dy \\ \sigma(x) &= -\alpha_i(x) + \frac{1}{2E}\frac{dE}{dx} \\ N(x) &= \int_{x_0}^{x} \sigma(\xi) d\xi = \log\left(\frac{A}{A_0}\right). \end{aligned} \qquad [3]$$

The N-Factor N refers to the logarithm of the amplitude change of a disturbance with initial amplitude A_0, calculated using the integrated growth rate σ, based on disturbance kinetic energy E, which is evaluated to the edge of the boundary layer y_e. The integral defining N is evaluated starting from the neutral point where the imaginary growth rate first becomes negative as the lower bound. The critical N-Factor (N_{crit}) is the value of the N-Factor where transition would be expected to occur based on experimental correlations. When α_i is negative, the associated eigenmode is unstable.

For CNE or TNE models, additional equations for species mass conservation are necessary to calculate the species mass fractions and their disturbances, and for TNE an additional energy equation is necessary. The continuity and momentum equations remain unchanged, using mixture values for ρ, p, and μ. These equations can be found in works by MacCormack and Candler [36], Chang et al. [20] and Anderson [37], as well as in previous work by the authors [30].

When thermal equilibrium is assumed, this means that the vibrational, electron, translational, and rotational energies had equilibrated and a single temperature is sufficient. In other words, we assume that the relaxation time between these energy modes is sufficiently shorter than the time scale of the flow phenomena. This is not necessarily true for hypersonic problems. For thermal nonequilibrium, multiple temperatures are required. In this work, we will use a two-temperature model for TNE, where the vibrational-electronic energies are associated with $T_V = T_{vib} = T_{el}$, where T_{el} refers to the electron translational-rotational temperature. The translational-rotational energy for all other species is associated with $T = T_{trans} = T_{rot}$. As compared to thermal equilibrium with CNE, an additional equation and variable are added to the system, with the associated disturbance T'_V. In addition, the chemistry model will take into account different rate controlling temperatures based on T and T_V depending on what type of reaction is occurring.

2.2 *Chemical Rates and Thermodynamic Properties*

A number of the quantities needed for boundary layer stability are dependent on the gas composition, including species production rates $\dot{\omega}_s$, transport properties viscosity and thermal conductivity, and thermodynamic quantities of specific heats and enthalpy. The equations implemented in LASTRAC to accommodate these models have been described previously [30]. This section will summarize which models were selected and address the relaxation time model.

The chemistry model used in this work is similar to that developed by Thompson et al. [38] for the calculation of thermodynamic and transport properties, with modifications to the curve fits used and additional data introduced to accommodate Martian atmospheric composition. The chemistry model used in this work uses the Chemical Equilibrium with Applications (CEA) [39] format for thermodynamic curve

fit coefficients, with the equations for specific heat, enthalpy, and entropy for each species from McBride et al. [40].

In addition to the thermodynamic quantities, transport quantities of viscosity, thermal conductivity, and diffusion coefficients are required. These quantities are calculated as functions of collision integrals between all pairs of chemical species included in the model. The collision integrals or collision cross-sections $\pi\bar{\Omega}_{i,j}^{(l,s)}$ for momentum transfer are defined as integrated functions of the differential cross section for the pair of species, the relative velocity and reduced velocities of the colliding particles, and the scattering angle. This equation can be found in Yos [41], and rather than evaluate the detailed expression for the collision cross-section at each temperature, curve fits based on cross-section values evaluated at a range of temperatures are used commonly in literature [42, 43]. Coefficients for curve fits for a CO_2-based five-species mixture were calculated using tabulated values from Wright et al. [44], using minimization of the mean square difference with the tabulated values. According to collision integral data tabulated in by Wright [44], the uncertainty in the values of the collision integrals ranges anywhere from $\pm 5\%$ to $\pm 50\%$, and so although a curve fit can match the data closely, it should not be expected to be any more accurate than the data used.

The modified Arrhenius equations are used to calculate reaction rates used to produce the species production rate $\dot{\omega}$, with the rate-controlling temperature T_c determined by the type of reaction. $T_c = \sqrt{TT_V}$ as used by Park [26,45] for dissociation reactions and $T_c = T$ for heavy molecule collision reactions. In this work, the coefficients for the modified Arrhenius equations are drawn from Park [26]. Noncatalytic boundary conditions are used at the surface in both mean flow and disturbance equations.

Although ionization and radiation effects are expected to be significant for reentry applications, these effects are neglected in the current work due to the increased complexity and computational cost. These effects may be included in the future. Effects of ablation and chemical reactions with ablation products are also neglected. Ionization, ablation, and three-temperature models are outside the scope of this work, where the next reasonable step to increase complexity and accuracy would be the addition of ionization effects.

The vibrational-translational energy relaxation time for diatomic molecules is found using the Millikan-White correlation [46] and a collision cross-section correction by Park [47]:

$$
\begin{aligned}
<\tau_s> &= \tau_s^{MW} + \begin{cases} \tau_s^P & T > 8000\,K \\ 0 & T < 8000\,K \end{cases} \\
\tau_s^{MW} &= \frac{1}{p_{atm}} \frac{\sum_{i=1,\neq e^-}^{N_s} n_i e^{A_s\left(T^{1/3}-0.015\mu_{si}^{1/4}\right)-18.42}}{\sum_{i=1,\neq e^-}^{N_s} n_i} \\
\tau_s^P &= (\sigma_s \bar{c}_s n_s)^{-1} \\
\bar{c}_s &= \sqrt{(8k_BT/\pi(M_s/Av))}\,,
\end{aligned}
\qquad [4]
$$

where τ_s^{MW} is the Millikan and White [46] semiempirical correlation, and τ_s^P is the Park [47] correction, using $\sigma_s = 10^{-16}\,cm^2$ as used by Gnoffo [43], Av is Avogadro's number such that M_s/Av is the mass per particle of species s in kg, and $n_s = C_s/M_s$ is the number density per species. We use τ_s directly rather than an averaged term as described by Gnoffo [43]. For molecules with multiple vibrational modes, specifically CO_2, we use a form of the Landau-Teller equation based on the number of vibrational modes and the characteristic vibrational temperatures. The production of vibrational energy due to the creation and destruction of diatomic molecules is accounted for in the vibrational-electronic energy equation using the species production rate $\dot{omega}_s$, and the vibrational energy per unit mass of the molecules $\hat{D}_s$. The approximation suggested by Park [48], $\hat{D}_s = \tilde{D}_s - k_BT$, is used with the dissociation energy $\tilde{D}_s$ taken from tabulated values. This makes the assumptions that there is preferential dissociation and recombination of the molecules in the higher vibrational states, and that the vibrational energy removed by dissociation differs by the average translational energy.

The relaxation time for a species s given vibrational mode j with characteristic temperature θ_j and reduced mass $\mu_{s,k}$ of the species and the colliding molecule k from Millikan and White [46] using Landau Teller theory is,

$$
\begin{aligned}
&\ln(p\tau_{s,j,k}) = \\
&(1.16\times 10^{-3})\mu_{s,k}^{\frac{1}{2}}\theta_j^{\frac{4}{3}}\left(T^{\frac{-1}{3}} - 0.015\mu_{s,k}^{\frac{1}{4}}\right) - 18.42\,,
\end{aligned}
\qquad [5]
$$

where we take the averaged relaxation time for vibrational mode j of species s in a mixture of N_s species as:

$$
\tau_{s,j} = \sum_{k=1}^{N_s} (\tau_{s,j,k}\rho_k) \,/\, \sum_{N=1}^{n_s} \rho_k\,. \qquad [6]
$$

The vibrational specific heat can be expressed in terms of the energy mode characteristic temperatures

as:

$$C^s_{v,V} = \frac{R_u}{M_s}\left(\frac{\theta_j}{T}\right)^2 \frac{e^{(-\theta_j/T)}}{\left(1-e^{(-\theta_j/T)}\right)^2}. \quad [7]$$

This leads to an expression for the vibrational-translational energy relaxation term for N_v vibrational modes with degeneracy g_j,

$$\frac{e^*_{v,s} - e_{v,s}}{<\tau_s>} = \sum_{j=1}^{N_v} \frac{g_j \theta_j}{\tau_{s,j}} \frac{R_u}{M_s} \left(\left(e^{\left(\frac{\theta_j}{T}\right)} - 1 \right)^{-1} - \left(e^{\left(\frac{\theta_j}{T_V}\right)} - 1 \right)^{-1} \right) \quad [8]$$

where this term is incorporated into the vibrational-electronic energy conservation equation, which can be found described further by Gnoffo [43] and in previous work [30–32].

2.3 *Mean flow calculations*

LAURA version 5.5-65135 [49] was used to produce the three-dimensional mean flow solutions, using a multiblock structured mesh. In order to produce mean flow solutions appropriately for boundary layer stability analysis, mesh dimensions with 257 points normal to the surface were used, based on the mesh convergence shown in Chang et al. [9]. The mesh adaptation to capture the shock and initial adaptation to the boundary layer thickness uses LAURA built-in adaptation utilities, and a further custom mesh adaptation was then applied in order to achieve a boundary layer mesh distribution appropriate to boundary layer stability calculations. This adaptation incorporated 150 points within the boundary layer, with 30 points inside the wall layer. The flow conditions described in Section 1.1 were applied using the freestream velocity, density, and temperature as listed.

For stability calculations the flow solution is interpolated to boundary layer profiles normal to the surface at points defined on a one-block, 401x201 surface mesh. This analysis proceeds similarly to what was done by Chang et al. [9]. The gas chemistry model described in the previous section applies to the stability analysis, which differs somewhat from the models used in LAURA 5. The effect of these differences is neglected in this work.

3. Results

3.1 *Mean Flow Solutions*

With the mesh adapted to the boundary layer and shock as described in Section 2.3, the boundary layer edge conditions are taken at a constant index from the volume solution mesh. These edge conditions are illustrated in Figure 1 and Figure 2.

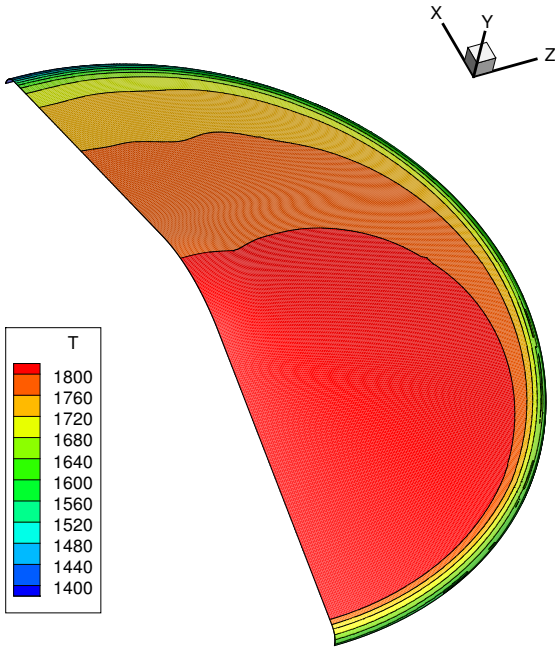

Fig. 1: Boundary layer edge translational temperature in Kelvin.

Given this flow field, we can expect Tollmien-Schlichting waves in the subsonic region along the symmetry plane, evolving into first mode waves in the supersonic region. Crossflow instabilities are not expected due to the relatively low crossflow Reynolds number off the symmetry plane shown in Figure 2. Since the measurements in the experiments are along the symmetry plane, we focus our analysis on the same region.

3.2 *Instabilities Along the Symmetry Plane*

Taking a point on the leeward side of the geometry, illustrated in Figure 2, we evaluate the local instabilities at a range of frequencies shown in Figure 3 and Figure 4, at the location indicated as x/R = 0.4987 in Figure 2, or a distance of 0.4987 of the radius in the x coordinate direction, where x = 0 at the nose. The optimized growth rates and associated wave angle are illustrated in this plot, showing the most unstable frequencies. Where the wave angle is close to zero, this is a 'two-dimensional' mode, while if it is close to 60°, it is an oblique mode. From this plot, we can observe that as the frequency increases there

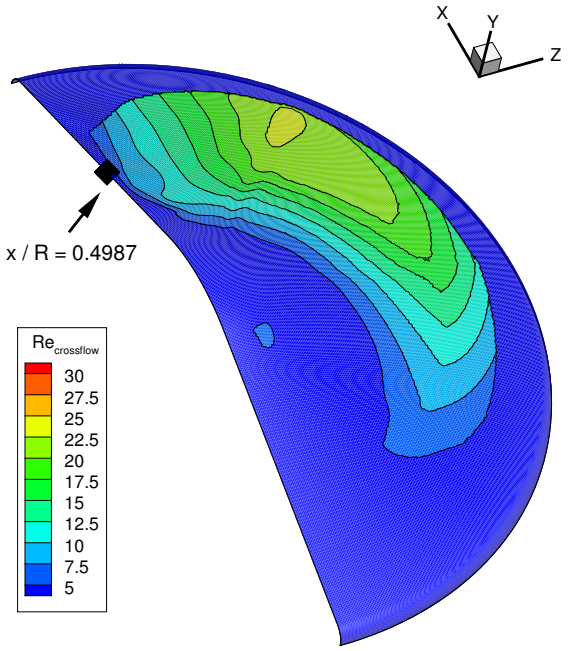

Fig. 2: Crossflow Reynolds number computed over the surface.

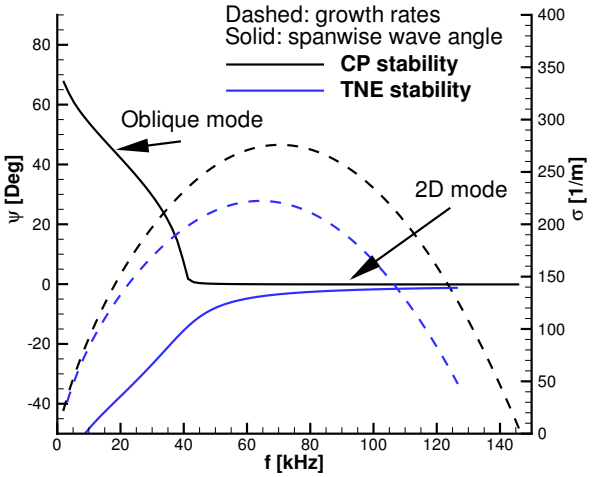

Fig. 3: Growth rate and optimized spanwise wave angle versus streamwise disturbance frequency at x/R of 0.4987. Both solutions use the same TNE mean flow.

is a smooth transition from the oblique mode to the two-dimensional mode at higher frequencies and remains two-dimensional at frequencies above 70 kHz. The instabilities are analyzed with both CP and TNE assumptions, using the same TNE mean flow. The effect of including TNE in the stability equations here is stabilizing, and modifies the spanwise wave angle. The spanwise wavelength, λ is shown in Figure 4, and we can see a distinct change in its value between the oblique and two-dimensional modes. The edge Mach number is approximately 0.9 at this location, which along with the location along the symmetry plane indicating that these are modified Tollmien-Schlichting waves, possibly a mixture of shear layer and Tollmien-Schlichting waves.

Figure 5 and Figure 6 illustrate the LST N-Factor and growth rate solutions at three frequencies. As identified in Figure 3, the frequencies in the 40-50 kHz range are associated with a mildly oblique mode while the 70 kHz mode is two-dimensional. The CP results shift to an oblique mode at a slightly lower frequency. The spanwise wave number is optimized for the largest growth rate at each point, giving a worst-case scenario but potentially introducing jumps between modes. As seen in Figure 6, although the two-dimensional mode is more unstable midway along the

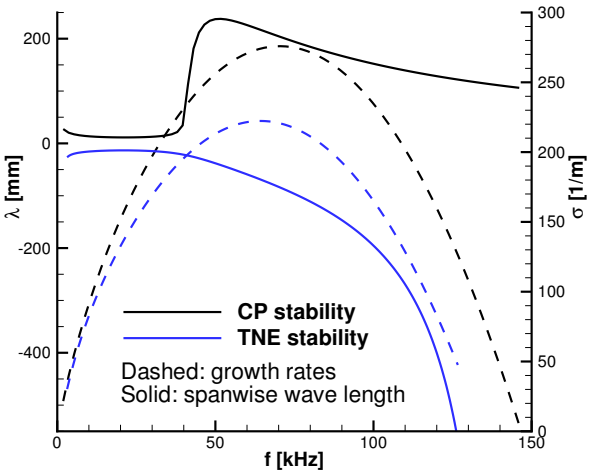

Fig. 4: Growth rate and optimized spanwise wave length versus streamwise disturbance frequency at x/R of 0.4987. Both solutions use the same TNE mean flow.

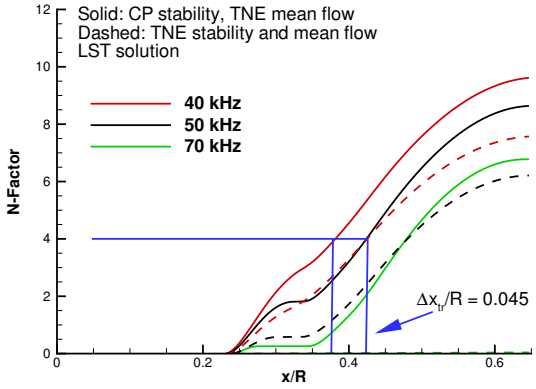

Fig. 5: N-Factor from the LST solution for disturbance frequencies of 40 – 70 kHz with optimized streamwise wave number.

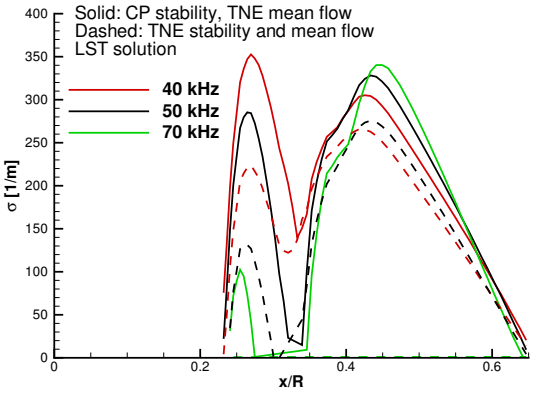

Fig. 6: Growth rates from the LST solution for disturbance frequencies of 40 – 70 kHz with optimized streamwise wave number.

surface, the oblique mode is more dominant upstream and leads to a higher overall N-Factor in Figure 5. Stability results are shown using both TNE and CP assumptions, both using the same TNE mean flow solution. The effect of TNE is slightly stabilizing, and, as shown in Figure 5 for the 40 kHz disturbance, the transition location assuming a critical N-Factor of 4 would be predicted to be 0.045 of the radius downstream of the transition location predicted assuming calorically perfect stability equations. Figure 7 illustrates the phase speeds for these same conditions. The phase speed is shifted slightly downward with the inclusion of TNE in the stability equations. The solutions are truncated at x/R of 0.65, and past this location the solution jumped to a different, neutrally stable, mode. This behavior is typical of shear layer instabilities.

Figure 8 shows the 40 kHz N-Factor curve from the LST solution with TNE shown in Figure 5, superimposed on the geometry with contours of crossflow Reynolds number. In wind tunnel tests, an N-Factor of 4 is often associated with transition onset. The N-Factors rise above 4 around halfway along the leeward side of the geometry, consistent with the behavior seen in Reference 34. The low crossflow Reynolds numbers off the symmetry plane indicate that crossflow instabilities would not be expected to be significant in this case.

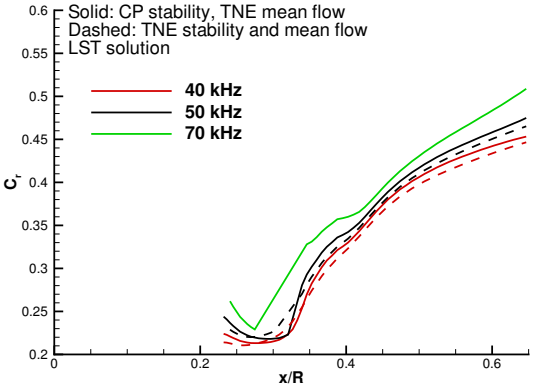

Fig. 7: Phase speed from the LST solution for disturbance frequencies of 40 – 70 kHz with optimized streamwise wave number.

4. Discussion

The stability results shown here are consistent with transition occurring on the leeward side of this case. Although direct comparison with experiment

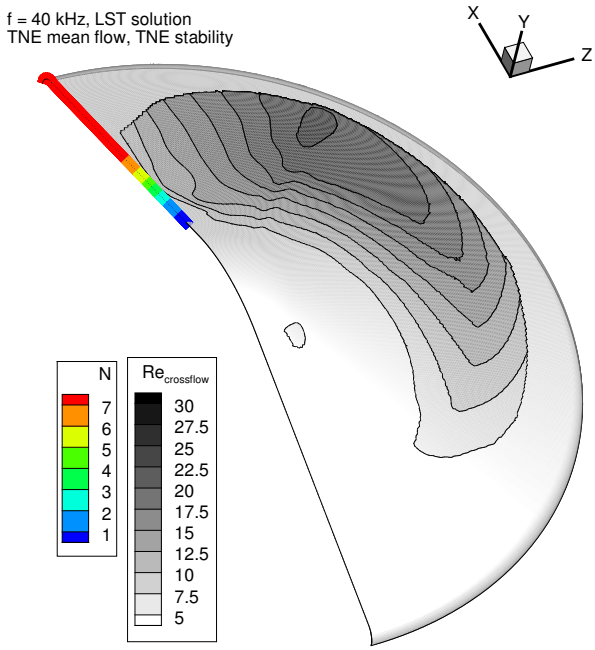

Fig. 8: Crossflow Reynolds number and N-Factor curves along centerline and streamlines for a streamwise disturbance frequency of 40 kHz.

is difficult due to the experimental results being produced at conditions outside of those normally used in the LENS-XX tunnel, the instability analysis conducted here with LASTRAC indicates that these conditions would have experienced transition due to modified Tollmien-Schlichting waves. Comparing to the data from Hollis [34], the critical N-Factor is approximately 4. Based on the crossflow Reynolds numbers off the symmetry plane, we would not expect crossflow instabilities off the symmetry plane in this case. Comparing between the predictions with CP stability equations and TNE stability equations, a change in the predicted transition location of around 4.5% of the geometry radius is shown at a fixed frequency, with LST model assumptions.

5. Conclusions

The results shown here demonstrate capabilities newly implemented in LASTRAC, of three-dimensional, thermochemical nonequilibrium boundary layer stability analysis. We are able to produce stability results for a geometry and conditions previously seen to be transitional in wind-tunnel experiments. The instabilities analyzed here are consistent with the transition on the leeward symmetry plane of the MSL geometry in CO_2. We also show the effect of TNE on modified Tollmien-Schlichting waves, which to the authors' knowledge, has not previously been examined in literature. The effect of TNE on the stability solution while holding the mean flow constant is generally stabilizing to both the oblique and two-dimensional waves. Since the effect of including TNE in the analysis is stabilizing, and leads to a small change in transition location relative to the currently-used technique of assuming fully turbulent flow, CP stability with TNE mean flow may be sufficient for design purposes, under the caveat that ionization and radiation effects were neglected in this analysis.

6. Acknowledgments

This work was funded under NASA contract number NNL13A08B, task orders NNL17AA56T and 80LARC18F0084, supported by the Hypersonics Technology Project in the Aeronautics Mission Directorate. The authors would also like to thank Dr. Hollis and Ms. Lee-Rausch for their help in editing and reviewing this paper.

References

[1] Wise, A., Prabhu, D. K., Johnston, C. O., Saunders, D. A., and Edquist, K. T., "Computational Aerothermodynamic Environments for the Mars 2020 Entry Capsule," *2018 Joint Thermophysics and Heat Transfer Conference*, (AIAA Paper 2018-3116), 2018.

[2] Whitehead, Jr., A., "NASP Aerodynamics," *National Aerospace Plane Conference, Meeting Paper Archive*, (AIAA Paper 1989-5013), July 1989.

[3] Kimmel, R., "Aspects of Hypersonic Boundary Layer Transition Control," *41st Aerospace Sciences Meeting and Exhibit, Aerospace Sciences Meetings*, (AIAA Paper 2003-772), Jan. 2003.

[4] Mack, L. M., "Boundary-Layer Linear Stability Theory," Tech. rep., California Institute of Technology Jet Propulsion Laboratory, 1984.

[5] Zanus, L., Miró Miró, F., and Pinna, F., "Nonlinear Parabolized Stability Analysis of Hypersonic Flows in Presence of Curvature Effects," *2018 AIAA Aerospace Sciences Meeting, AIAA SciTech Forum*, (AIAA Paper 2018-2087), Jan. 2018.

[6] Unnikrishnan, S. and Gaitonde, D. V., "Kovasznay-Type Analysis of Transition Modes in a Hypersonic Boundary Layer," *2018 AIAA Aerospace Sciences Meeting, AIAA SciTech Forum*, (AIAA Paper 2018-2086), Jan. 2018.

[7] Lakebrink, M. T., Paredes, P., and Borg, M. P., "Toward Robust Prediction of Crossflow-Wave Instability in Hypersonic Boundary Layers," *Computers & Fluids*, Vol. 144, 2017, pp. 1 – 9.

[8] Moyes, A. J., Paredes, P., Kocian, T. S., and Reed, H. L., "Secondary Instability Analysis of Crossflow on a Hypersonic Yawed Straight Circular Cone," *Journal of Fluid Mechanics*, Vol. 812, 2017, pp. 370–397.

[9] Chang, C.-L., Choudhari, M., Hollis, B., and Li, F., "Transition Analysis for the Mars Science Laboratory Entry Vehicle," *41st AIAA Thermophysics Conference*, (AIAA Paper 2009-4076), 2009.

[10] Kennedy, R. E., Laurence, S. J., Smith, M. S., and Marineau, E. C., "Visualization of the Second-Mode Instability on a Sharp Cone at Mach 14," *2018 AIAA Aerospace Sciences Meeting, AIAA SciTech Forum,*, (AIAA Paper 2018-2083), Jan. 2018.

[11] Hollis, B., Liechty, D., Wright, M., Holden, M., Wadhams, T., MacLean, M., and Dyakonov, A., "Transition Onset and Turbulent Heating Measurements for the Mars Science Laboratory Entry Vehicle," *43rd AIAA Aerospace Sciences Meeting and Exhibit, Aerospace Sciences Meetings*, (AIAA Paper 2005-1437), Jan. 2005.

[12] Johnson, H. and Candler, G., "PSE Analysis of Reacting Hypersonic Boundary Layer Transition," *30th Fluid Dynamics Conference, Fluid Dynamics and Co-located Conferences*, (AIAA Paper 1999-3793), June 1999.

[13] Johnson, H. and Candler, G., "Hypersonic Boundary Layer Stability Analysis Using PSE-Chem," *35th AIAA Fluid Dynamics Conference and Exhibit, Fluid Dynamics and Co-located Conferences*, (AIAA Paper 2005-5023), June 2005.

[14] Johnson, H., Candler, G., and Alba, C., "Three-Dimensional Hypersonic Boundary Layer Stability Analysis with STABL-3D," *40th Fluid Dynamics Conference and Exhibit, Fluid Dynamics and Co-located Conferences*, (AIAA Paper 2010-5005), June 2010.

[15] Bertolotti, F. P., "The Influence of Rotational and Vibrational Energy Relaxation on Boundary-Layer Stability," *Journal of Fluid Mechanics*, Vol. 372, 1998, pp. 93–118.

[16] Wang, X., "Passive Control of Hypersonic Non-Equilibrium Boundary Layers using Regular Porous Coating," *47th AIAA Fluid Dynamics Conference, AIAA AVIATION Forum*, (AIAA Paper 2017-4519), June 2017.

[17] Knisely, C. P. and Zhong, X., "Supersonic Modes in Hot-Wall Hypersonic Boundary Layers with Thermochemical Nonequilibrium Effects," *2018 AIAA Aerospace Sciences Meeting, AIAA SciTech Forum,*, (AIAA Paper 2018-2085), Jan. 2018.

[18] Miró Miró, F., Pinna, F., Beyak, E. S., Barbante, P., and Reed, H. L., "Diffusion and Chemical Non-Equilibrium Effects on Hypersonic Boundary-Layer Stability," *2018 AIAA Aerospace Sciences Meeting, AIAA SciTech Forum,*, (AIAA Paper 2018-1824), Jan. 2018.

[19] Malik, M. R., "Hypersonic Flight Transition Data Analysis Using Parabolized Stability Equations with Chemistry Effects," *Journal of Spacecraft and Rockets*, Vol. 40, No. 3, May 2003, pp. 332–344.

[20] Chang, C.-L., Vinh, H., and Malik, M., "Hypersonic Boundary-Layer Stability with Chemical Reactions Using PSE," *28th Fluid Dynamics Conference, Fluid Dynamics and Co-located Conferences*, (AIAA Paper 1997-2012), June 1997.

[21] Wartemann, V., Wagner, A., Wagnild, R., Pinna, F., Miró Miró, F., Tanno, H., and Johnson, H., "High-Enthalpy Effects on Hypersonic Boundary-Layer Transition," *Journal of Spacecraft and Rockets*, Vol. 56, No. 2, 2018, pp. 347–356.

[22] Hollis, B. R., Prabhu, D. K., Maclean, M., and Dufrene, A., "Blunt-Body Aerothermodynamic Database from High-Enthalpy Carbon-Dioxide Testing in an Expansion Tunnel," *Journal of Thermophysics and Heat Transfer*, Vol. 31, No. 3, 2017, pp. 712–731.

[23] Edquist, K. T., Hollis, B. R., Johnston, C. O., Bose, D., White, T. R., and Mahzari, M., "Mars Science Laboratory Heat Shield Aerothermodynamics: Design and Reconstruction," *Journal of Spacecraft and Rockets*, Vol. 51, No. 4, July 2014, pp. 1106–1124.

[24] Johnson, H., Candler, G., and Wright, M., "Boundary Layer Stability Analysis of Mars Science Laboratory Aeroshell," *44th AIAA Aerospace Sciences Meeting and Exhibit*, (AIAA Paper 2006-920), 2006.

[25] Edquist, K., Liechty, D. S., Hollis, B. R., Alter, S. J., and Loomis, M. P., "Aeroheating Environments for a Mars Smart Lander," *Journal of Spacecraft and Rockets*, Vol. 43, No. 2, March 2006, pp. 330–339.

[26] Park, C., Howe, J. T., Jaffe, R. L., and Candler, G. V., "Review of Chemical-Kinetic Problems of Future NASA Missions. II - Mars Entries," *Journal of Thermophysics and Heat Transfer*, Vol. 8, No. 1, Jan. 1994, pp. 9–23.

[27] Jewell, J., Wagnild, R., Leyva, I., Candler, G., and Shepherd, J., "Transition Within a Hypervelocity Boundary Layer on a 5-Degree Half-Angle Cone in Air/CO2 Mixtures," *51st AIAA Aerospace Sciences Meeting Including the New Horizons Forum and Aerospace Exposition*, (AIAA Paper 2013-0523), 2013.

[28] Wagnild, R., Candler, G., Leyva, I., Jewell, J., and Hornung, H., "Carbon Dioxide Injection for Hypervelocity Boundary Layer Stability," *48th AIAA Aerospace Sciences Meeting Including the New Horizons Forum and Aerospace Exposition*, (AIAA Paper 2010-1244), 2010.

[29] Leyva, I., Laurence, S., Beierholm, A., Hornung, H., Wagnild, R., and Candler, G., "Transition Delay in Hypervelocity Boundary Layers by Means of CO2/Acoustic Instability Interactions," *47th AIAA Aerospace Sciences Meeting including The New Horizons Forum and Aerospace Exposition*, (AIAA Paper 2009-1287), 2009.

[30] Kline, H., Chang, C.-L., and Li, F., "Hypersonic Chemically Reacting Boundary-Layer Stability using LASTRAC," *2018 Fluid Dynamics Conference*, (AIAA Paper 2018-3699), 2018.

[31] Kline, H., Chang, C.-L., and Li, F., "Boundary Layer Stability and Transition in a Chemically Reacting Martian Atmosphere using LASTRAC," *22nd AIAA International Space Planes and Hypersonics Systems and Technologies Conference*, (AIAA Paper 2018-5206), 2018.

[32] Kline, H., Chang, C.-L., and Li, F., "Multiple Boundary Layer Instability Modes with Nonequilibrium and Wall Temperature Effects Using LASTRAC," *AIAA Aviation 2019 Forum*, (AIAA Paper 2019-2850), 2019.

[33] Chang, C.-L., "Langley Stability and Transition Analysis Code (LASTRAC) Version 1.2 User Manual," NASA TM- 2004-213233, NASA, June 2004.

[34] Hollis, B. R., Prabhu, D. K., Maclean, M., and Dufrene, A., "Blunt-body aerothermodynamic database from high-enthalpy CO2 testing in an expansion tunnel," *46th AIAA Thermophysics Conference*, (AIAA Paper 2016-4151), 2016.

[35] Chang, C.-L., "LASTRAC. 3d: Transition prediction in 3D boundary layers," *34th AIAA Fluid Dynamics Conference and Exhibit*, (AIAA Paper 2004-2542), 2004.

[36] Candler, G. V. and Maccormack, R. W., "Computation of Weakly Ionized Hypersonic Flows in Thermochemical Nonequilibrium," *Journal of Thermophysics and Heat Transfer*, Vol. 5, No. 3, July 1991, pp. 266–273.

[37] Anderson, J. D., *Hypersonic and High Temperature Gas Dynamics*, AIAA education series, AIAA, Reston, Va, 2nd ed., 2006, OCLC: 255373855.

[38] Thompson, R. A., Lee, K.-P., and Gupta, R. N., "Computer Codes for the Evaluation of Thermodynamic Properties, Transport Properties, and Equilibrium Constants of an 11-Species Air Model," NASA TM- 102602, NASA, 1990.

[39] "Chemical Equilibrium with Applications," `https://www.grc.nasa.gov/www/CEAWeb/`, 2016 (last accessed 07/20/2018).

[40] McBride, B. J., Zehe, M. J., and Gordon, S., "NASA Glenn Coefficients for Calculating Thermodynamic Properties of Individual Species," NASA TP- 2002-211556, NASA, 2002.

[41] Yos, J. M., "Transport Properties of Nitrogen, Hydrogen, Oxygen, and Air to 30,000 K," RAD TM- 63-7, AVCO Corp., 1963.

[42] Gupta, R. N., Yos, J. M., Thompson, R. A., and Lee, K.-P., "A Review of Reaction Rates and Thermodynamic and Transport Properties for an 11-Species Air Model for Chemical and Thermal Nonequilibrium Calculations to 30000 K," NASA RP- 1232, NASA, 1990.

[43] Gnoffo, P. A., Gupta, R. N., and Shinn, J. L., "Conservation Equations and Physical Models for Hypersonic Air Flows in Thermal and Chemical Nonequilibrium," NASA TP- 2867, NASA, 1989.

[44] Wright, M. J., Hwang, H. H., and Schwenke, D. W., "Recommended Collision Integrals for Transport Property Computations Part II: Mars and Venus Entries," *AIAA Journal*, Vol. 45, No. 1, Jan. 2007, pp. 281–288.

[45] Park, C., "Assessment of Two-Temperature Kinetic Model for Ionizing Air," *Journal of Thermophysics and Heat Transfer*, Vol. 3, No. 3, 1989, pp. 233–244.

[46] Millikan, R. C. and White, D. R., "Systematics of Vibrational Relaxation," *The Journal of Chemical Physics*, Vol. 39, No. 12, 1963, pp. 3209–3213.

[47] Park, C., "Problems of Rate Chemistry in the Flight Regimes of Aeroassisted Orbital Transfer Vehicles," *Progress in Astronautics and Aeronautics*, Vol. 96, 1985, pp. 511–537.

[48] Park, C., "Two-Temperature Interpretation of Dissociation Rate Data for N2 and O2," *26th Aerospace Sciences Meeting*, 1988, p. 458.

[49] Mazaheri, A., Gnoffo, P. A., Johnston, C. O., and Kleb, W. L., "LAURA Users Manual: 5.5-64987," NASA TM-, 2013.